CMS Physics Analysis Summary

Contact: cms-pag-conveners-susy@cern.ch 2011/11/28

Search for Physics Beyond the Standard Model in Events with Opposite-sign Tau Pairs and Missing Energy

The CMS Collaboration

Abstract

A search for physics beyond the Standard Model with highly energetic jets, large momentum imbalance, and opposite-sign tau pairs in the final state is performed using data samples with integrated luminosities of 1 fb^{-1} of pp collisions at $\sqrt{s} =$ 7 TeV collected with the CMS detector at the LHC at CERN. The Standard Model backgrounds are estimated using data–driven techniques. The number of observed events is in good agreement with the predictions for Standard Model background processes and upper limits are set in the context of models of supersymmetry.

1 Introduction

The analysis presented in this paper is a search for physics beyond the standard model (BSM) using data collected with the Compact Muon Solenoid (CMS) in proton-proton collisions at a center of mass energy of $\sqrt{s} = 7$ TeV at the Large Hadron Collider (LHC). The data samples correspond to an integrated luminosity of 1 fb^{-1}.

The motivations for physics beyond the SM range from astrophysical evidence of dark matter (DM) to theoretical issues associated with the observation of certain particle mass heirarchies. Since new particles predicted by many BSM physics processes have not been observed by previous experiments, our search concentrates on heavy BSM particle production. Focus is placed on strongly produced BSM processes with a large enough cross section to be observed with the current dataset. Additionally, astrophysical evidence for dark matter points to the existence of weakly-interacting massive particles at the scale of electroweak symmetry breaking [1]. These particles, if produced in proton-proton collisions at the LHC, would escape detection and result in a significant momentum imbalance in the detector. This analysis focuses on production of heavy colored particles followed by cascade decays leading to final states with leptons. The couplings to third generation leptons can be enhanced, thus leading to final states that predominantly contain tau leptons. Therefore, the analysis presented is a general BSM search in events with jets, large momentum imbalance in the detector, and opposite sign dilepton final states including one or more hadronically decaying τ leptons.

The analysis presented is not limited to a particular BSM theory. However, to illustrate the sensitivity of this search for BSM processes, the constrained minimal supersymmetric extension of the standard model (cMSSM) is chosen as a benchmark due to the simplicity of the model [2–5]. The cMSSM contains only five parameters to determine all the masses and couplings: m_0 (universal sfermion mass), $m_{1/2}$ (universal gaugino mass), A_0 (universal soft breaking trilinear coupling constant), tanβ (the ratio of vacuum expectation values of two Higgs doublets), and the sign of μ (the bilinear Higgs coupling constant). We use three sets of parameters, referred to as LM1, LM2, and LM13 [6], to illustrate the sensitivity to possible BSM processes. The parameter values for [LM1, LM2, LM13] are $m_0 = [60, 185, 270]$, $m_{1/2} = [250, 350, 218]$, tan$\beta = [10, 35, 40]$, $A_0 = [0, 0, -553]$, and $\mu > 0$.

2 Analysis Strategy

The tau is the heaviest known lepton with a mass of 1.777 GeV and a lifetime of 2.9×10^{-13} seconds. About one third of taus decay leptonically and the rest hadronically. In the latter case, τ_h candidates consist of final states with one, three, or (rarely) five charged mesons usually accompanied by up to two neutral pions. Throughout the text, the visible part of a hadronically decaying tau lepton will be referred to as τ_h. There are six distinct possible final states of di-tau decays, namely ee, $\mu\mu$, $e\mu$, $e\tau_h$, $\mu\tau_h$, and $\tau_h\tau_h$. Since it is difficult to distinguish ee, $\mu\mu$, and $e\mu$ final states from direct di-lepton production, these final states are studied separately [7].

The events with the $e/\mu + \tau_h$ (section 7) and $\tau_h\tau_h$ (section 8) final states are selected using different trigger requirements. The $e\tau_h$ and $\mu\tau_h$ final states are required to pass the lepton triggers and the $\tau_h\tau_h$ final states are required to pass a fully hadronic trigger based on $|\overrightarrow{\not{H}_T}|$quantity, where $\not{H}_T = |\overrightarrow{\not{H}_T}| = |-\sum_i \overrightarrow{p_T^i}|$, and the sum runs over all jets with transverse momenta $p_T > 30$ GeV. The events are required to have at least two jets. For the $e/\mu + \tau_h$ final states two signal regions are defined, one with large transverse energy imbalance, E_T^{miss}, and another one with large hadronic activities H_T, calculated as scalar sum of all PF jets transverse momenta with

$p_T > 30$ GeV. In the $\tau_h\tau_h$ case only one signal region is selected. Table 1 summarizes the signal regions and selection requirements. The SM backgrounds are estimated using data-driven techniques, which differs depending on the final state. We perform a counting experiment and compare the observed yields with the data-driven predictions for SM backgrounds.

Table 1: Summary of the selections and signal region definitions.

Property	$e/\mu\tau_h$ high E_T^{miss}	$e/\mu\tau_h$ high H_T	$\tau_h\tau_h$
Geom. Acceptance	$\|\eta^{e,\mu,\tau_h}\| < 2.1$		
Charge	opposite-sign		
Trigger	$e/\mu + \tau_h$		$\|\overrightarrow{\not{H}_T}\|$
Momentum	$p_T^{e,\mu,\tau_h} > 20$ GeV		$p_T^{\tau_h} > 15$ GeV
N_{jets}	2 jets ($p_T > 30$ GeV)		2 jets ($p_T > 100$ GeV)
Transverse Energy imbalance	$E_T^{miss} > 200$ GeV	$E_T^{miss} > 150$ GeV	$\|\overrightarrow{\not{H}_T}\| > 200$ GeV
Hadronic activity	$H_T > 300$ GeV	$H_T > 400$ GeV	—

3 CMS Detector

The CMS experiment [8] uses a right-handed coordinate system, with the origin at the nominal interaction point, the x-axis pointing to the center of the LHC ring, the y-axis pointing up (perpendicular to the LHC plane), and the z-axis along the anticlockwise-beam direction. The polar angle, θ, is measured from the positive z-axis and the azimuthal angle, ϕ, is measured in the x-y plane. The pseudorapidity is given by $\eta = -\ln(\tan\theta/2)$.

The central feature of the CMS apparatus is a superconducting solenoid, of 6 m inner diameter, providing a field of 3.8 T. Within the field volume are the silicon pixel and strip tracker, the crystal electromagnetic calorimeter (ECAL), which includes a silicon sensor preshower detector in front of the ECAL endcaps, and the brass/scintillator hadron calorimeter (HCAL). Muons are measured in gas-ionization detectors embedded in the steel return yoke. In addition to the barrel and endcap detectors, CMS has extensive forward calorimetry. The ECAL has an ultimate energy resolution of better than 0.5% for unconverted photons with transverse energies above 100 GeV. The energy resolution is 3% or better for the range of electron energies relevant for this analysis. The HCAL, when combined with the ECAL, measures jets with a resolution $\Delta E/E \approx 100\,\%/\sqrt{E[\mathrm{GeV}]} \oplus 5\,\%$.

The inner tracker measures charged particles within $|\eta| < 2.5$ and provides an impact parameter resolution of ~ 15 μm and a transverse momentum (p_T) resolution of about 1.5 % for 100 GeV particles. The relative luminosity is measured using the forward calorimeters. Collision events were selected by a first level trigger made of a system of fast electronics and a higher level trigger that consists of a farm of commercial CPUs running a version of the offline reconstruction optimized for fast processing. A more detailed description of the CMS detector can be found elsewhere [9].

4 Backgrounds and Samples

The major SM process where two taus with opposite charge are produced, $Z \to \tau\tau$, is heavily suppressed by the requirement of missing transverse momenta and significant hadronic activity. Other SM processes such as semileptonic and fully hadronic $t\bar{t}$, W, and Z production with associated jets contribute to the background when jets are misidentified as τ_h.

$Z \to \nu\bar{\nu}$ + jets can become a background for the $\tau_h\tau_h$ channel. The neutrinos from the Z boson decay give rise to large $E_{\mathrm{T}}^{\mathrm{miss}}$ and two jets are misidentified as τ_h. The low multiplicity of jets means the probability to obtain 2 tau-like jets and 2 additional high p_T jets is low. However, its contribution is highly dependent on the jet$\to \tau_h$ misidentification rate.

Collision data was compared to samples of simulated events. QCD di-jet, Drell-Yan, and SUSY samples are generated with PYTHIA [10], while the Madgraph [11] package has been used to model multi-jet processes such as W + jets, $Z \to \nu\bar{\nu}$ + jets, and $t\bar{t}$. The tau decays have been performed with TAUOLA [12]. The Monte Carlo generated events have been processed with a detailed simulation of the CMS apparatus using the GEANT4 package [13]. The MC yields are normalized to integrated luminosity using next-to-leading order (NLO) cross sections. At the LHC luminosity used in this analysis, the mean number of interactions in a single beam crossing is approximately 5. In the MC, multiple interactions are superimposed on the hard collision, and the MC is reweighted such that the distribution of reconstructed primary vertices matches that in data.

5 Object Reconstruction and Identification

The anti-k_T clustering algorithm [14] with $\Delta R = 0.5$ is used for jet clustering. The jets and transverse momentum imbalance in the detector ($E_{\mathrm{T}}^{\mathrm{miss}}$) are reconstructed with the Particle Flow (PF) algorithm [15]. Additionally, jets are required to pass jet identification criteria designed to reject anomalous behaviour from the calorimeters and be fairly well separated from the identified τ_h: $\Delta R(j, \tau_h) > 0.3$. In the e/μ+τ_h final states, the variable H_T is used to define a signal region with large amounts of hadronic activity. The quantity H_T is defined as $H_T = \sum_i p_T^i$, where i runs over all PF jets with $p_T > 30$ GeV.

Muons are reconstructed using the tracker and muon chambers. Quality cuts, based on the minimum number of hits in the silicon tracker, pixel detector, and muon chambers are applied to suppress backgrounds from punch-throughs and decays in flight.

Electrons are reconstructed by combining tracks produced by the Gaussian Sum Filter algorithm with ECAL clusters. Requirements in shower shape and track-ECAL matching are imposed to distinguish prompt electrons from charged pions mimicking electron signatures, and from electrons produced by photon conversions.

Because electrons and muons produced in the decays of low-mass particles, such as hadrons containing b and c quarks, are nearly always inside jets, they can be suppressed by requiring the light leptons to be isolated in space from other particles that carry a substantial amount of transverse momentum. The details of the light lepton isolation measurement are given in [16]. In brief, a cone of size ΔR is constructed around the lepton momentum direction. The lepton relative isolation is then quantified by summing the transverse energy (as measured in the calorimeters) and the transverse momentum (as measured in the silicon tracker) of all objects within this cone, excluding the lepton, and dividing by the lepton transverse momentum. The resulting quantity is required to be less than 0.15, rejecting the large background arising from QCD production of jets.

Isolated and identified electrons and muons must have $p_T > 20$ GeV and $|\eta| < 2.1$ and their identification and isolation criteria are identical to Ref. [7].

Hadronic tau decays (τ_h) are reconstructed with the Particle Flow (PF) algorithm [17] which is used to form a mutually-exclusive collection of reconstructed particles (muons, electrons, photons, charged and neutral hadrons) by combining tracks and calorimeter clusters. Tau re-

construction and identification is performed using the Hadrons Plus Strips (HPS) algorithm [18]. As part of this identification procedure loose isolation is applied for the $e/\mu + \tau_h$ final states. In order to increase the signal acceptance for the $\tau_h\tau_h$ final state, isolation thresholds are further increased and a smaller isolation cone size is used.

Isolated electrons and muons can easily be misidentified as hadronic taus. For this reason HPS taus are required to pass anti-electron selections and be incompatible with a muon signature in the muon system.

6 Acceptance and Efficiency Systematic Uncertainties

We have included sources of systematics such as trigger efficiencies, identification efficiencies, energy and momentum scale, luminosiy measurement [19], parton distribution functions and initial and final state radiation (Table 2). The systematic uncertainty in the lepton acceptance consists of two parts: the trigger efficiency uncertainty and the identification and isolation uncertainty. We verify that the simulation reproduces the lepton identification and isolation efficiencies in data using samples of $Z \to \ell\ell$; the data and simulation efficiencies are found to be consistent within 2% electrons or muons. The systematic uncertainty for the τ_h identification (6%) is obtained using a fit of data in a $Z \to \tau\tau$ enhanced region and fixing the cross section to that measured using $ee/\mu\mu$. This is further validated by obtaining a $Z \to \tau\tau$ enhanced region showing consistency between simulation and data. The uncertainty of the trigger efficiency (1%) of the lepton triggers is estimated with the tag and probe method [20]. Systematic uncertainties on the $\not{H}_T$ triggers (6.5%) are measured using a high purity sample of $t\bar{t}$ events which have a similar topology to the signal region. Tau and jet energy scale systematics also affect our knowledge of the mass shapes. The E_T^{miss} scale uncertainties contribute via the jet energy scale and unclustered energy scale. The impact of this uncertainty is final-state dependent. Final states characterized by very large hadronic activity and E_T^{miss} are less sensitive than final states where the E_T^{miss} and H_T are typically close to the minimum requirements applied to these quantities. To be more quantitative, we have used the method of Ref. [16] to evaluate the systematic uncertainties in the acceptance for $t\bar{t}$ and for the two benchmark SUSY points using a 7.5% uncertainty in the hadronic energy scale (Table 2). For the high E_T^{miss} (high H_T) signal region for $t\bar{t}$ the uncertainty is $\sim$60% ($\sim$50%). The signal acceptance and efficiency, as well as the systematic uncertainties, depend on the signal model. For some of the individual uncertainties, it is reasonable to quote values based on SM control samples with kinematic properties similar to the SUSY benchmark models. For others that depend strongly on the kinematic properties of the event, the systematic uncertainties must be quoted model by model. The systematic effect due to imprecise knowledge of the parton distribution functions (25%) is determined by comparing CTEQ6.6L[21], MSTW 2008 NLO [22] and NNPDF 2.1 [23] PDF with the default PDF. The systematic effect due to imprecise modeling of initial and final state radiation (3.1% for ISR and 2.5% for FSR) is determined by re-weighting events to account for effects such as missing α terms in the soft-collinear approach [24] and missing NLO terms in the parton shower approach [25].

7 Single Hadronic Tau Final State

7.1 Background Estimation

The e/μ τ_h channels are studied with an integrated luminosity of 0.98 fb^{-1}. The backgrounds are studied in a region, where all the final selection requirements are applied but the E_T^{miss} and

Table 2: Summary of the systematic uncertainties included for possible signal prediction

Source	$e/\mu\tau_h$ high E_T^{miss}	$e/\mu\tau_h$ high H_T	$\tau_h\tau_h$
$\tau_h$efficiency	6%		
Luminosity	4.5%		
PDF description	25%		
ISR description	3.1%		
FSR description	2.5%		
Light lepton efficiency	2%		–
Trigger efficiency	1%		6.5%
Jet energy scale (7.5%)	11% (LM1), 6% (LM2), 12% (LM13)	9% (LM1), 5% (LM2), 11% (LM13)	10% (LM1), 6% (LM2), 10% (LM13)

H_T requirements are relaxed to $E_T^{miss} > 100$ GeV, $H_T > 100$ GeV (Fig. 2). The data yields and MC predictions for the preselected region are summarized in Table 3.

As expected, the MC predicts that the sample passing the preselection is dominated by dilepton $t\bar{t}$, $Z \to \tau^+\tau^-$and non-prompt tau decays. The data yield is in reasonable agreement with the predictions. We also quote the yields for the LM1, LM2 and LM13 benchmark scenarios.

Table 3: Data yields and MC predictions after preselection, using NLO production cross sections. "$\sum$MC True" indicates the sum of SM backgrounds including a real τ_h decay, "$\sum$MC Fake" indicates SM processes with τ_h not associated to a τ in simulation and "$\sum$SM MC" is the sum of both contributions. The LM1, LM2 and LM13 benchmark scenarios are defined in the text. Uncertainties are marked as statistical and systematical.

Sample	$e\tau_h$	$\mu\tau_h$	total
$W \to l/\tau\nu$	12.5 ± 5.9	15.3 ± 5.8	27.8 ± 8.3
$Z \to ll$	2.2 ± 2.2	< 0.1	2.2 ± 2.2
$Z \to \tau\tau$	8.9 ± 4.0	12.4 ± 4.1	21.3 ± 5.7
$t\bar{t}$ + jets	45.9 ± 2.2	47.2 ± 2.1	93.1 ± 3.0
$\sum$MC True	36.0 ± 3.2	38.9 ± 3.9	$75.0 \pm 5.0_{stat.} \pm 24.4_{syst.}$
$\sum$MC Fake	33.6 ± 7.1	35.9 ± 6.3	$69.5 \pm 9.5_{stat.} \pm 22.6_{syst.}$
$\sum$MC SM	69.6 ± 7.8	74.9 ± 7.4	$144.5 \pm 10.7_{stat.} \pm 47.1_{syst.}$
Data	59	78	137
$LM1$	10.6 ± 0.6	15.5 ± 0.7	$26.1 \pm 0.9_{stat.} \pm 8.0_{syst.}$
$LM2$	1.8 ± 0.1	2.3 ± 0.1	$4.1 \pm 0.2_{stat.} \pm 1.2_{syst.}$
$LM13$	24.5 ± 2.1	41.2 ± 2.7	$65.7 \pm 3.4_{stat.} \pm 20.3_{syst.}$

Figure 1 compares several kinematic distributions in data and SM MC for events passing the preselection. As an illustration, we also show the MC distributions for the LM13 benchmark point. We find that the SM MC reproduces the properties of the bulk of data.

7.1.1 Top Background Estimation

The top-background is estimated with the dilepton transverse momentum ($p_T(\ell\ell)$) method, which is based on the idea [26] that in dilepton $t\bar{t}$ events the p_T distributions of the charged leptons and neutrinos from W decays are related, because of the common boosts from the top and W decays. This relation is governed by the polarization of the W's, which is well

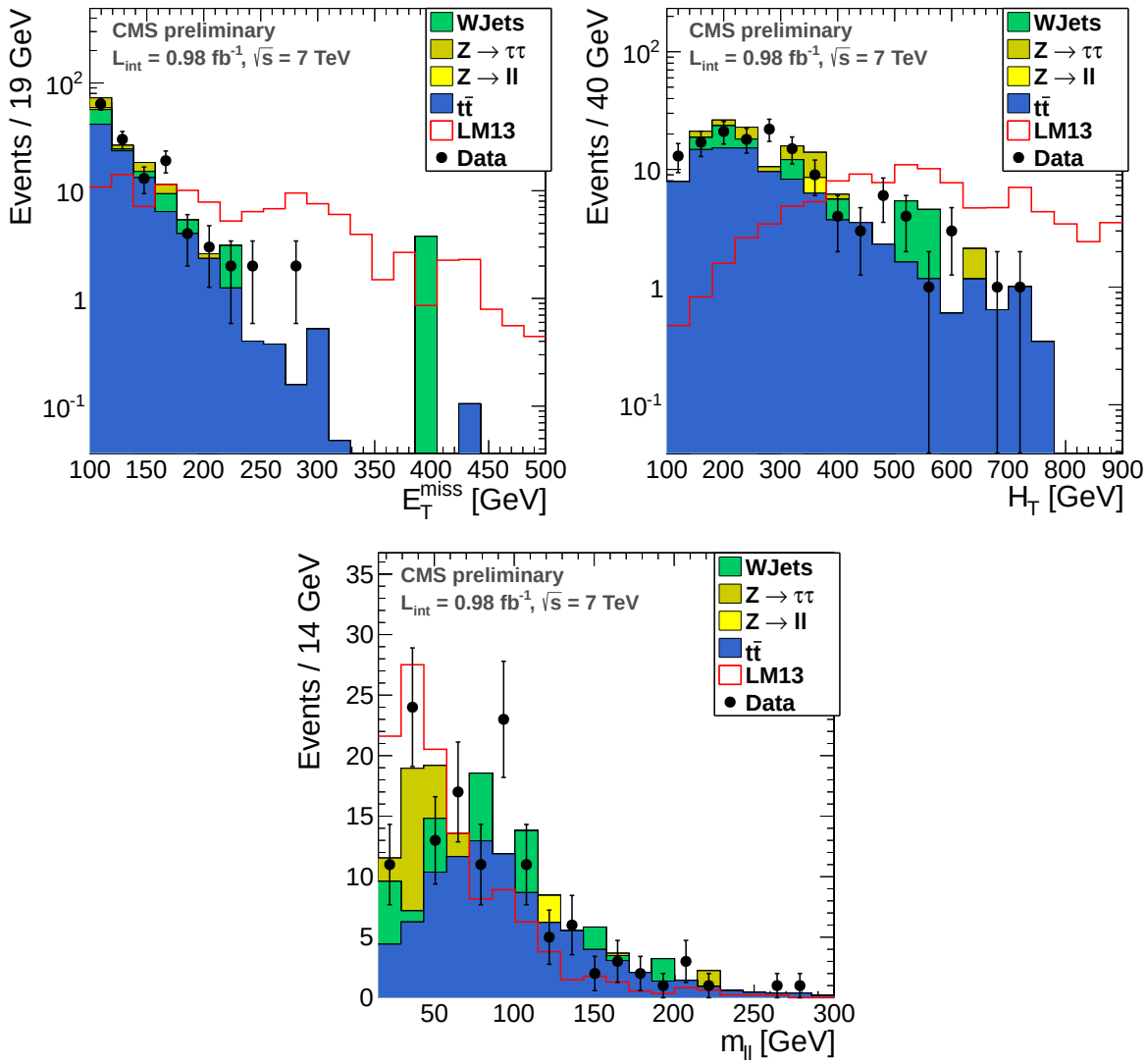

Figure 1: Distributions of (top left) missing tranverse energy $E_{\mathrm{T}}^{\mathrm{miss}}$, (top right) scalar sum of jet transverse energies (H_{T}), (bottom) dilepton invariant mass $m(\ell\ell)$ for SM MC and data after preselection. The MC distributions for the LM13 benchmark point are also shown.

understood in SM top decays [27, 28] and can therefore be reliably accounted for. We use the observed $p_{\mathrm{T}}(\ell\ell)$ distribution to model the $p_{\mathrm{T}}(\nu\nu)$ distribution, which is identified with $E_{\mathrm{T}}^{\mathrm{miss}}$.

The top-background in the ee, eμ, and $\mu\mu$ channels is estimated using the procedure described in [29]. For each signal region S, we count the number of events falling in the region S', which is defined using the same requirements as S but replacing the $E_{\mathrm{T}}^{\mathrm{miss}}$ requirement with a $p_T(\ell\ell)$ requirement. The contribution from Drell-Yan (DY) processes, estimated using the data-driven $R_{out/in}$ technique [7, 16], is subtracted from region S'. The number of top events in the signal region is estimated as:

$$n_{Top} = (n_{S'} - n_{DY}) \times K_{50} \times K_C \times K_\tau. \quad (1)$$

where factors K are the scaling factors between S′ and S regions . The first correction accounts for the fact that we require $E_{\mathrm{T}}^{\mathrm{miss}} > 50$ GeV in the preselection but there is no corresponding

requirement on $p_T(\ell\ell)$; this correction is measured from data to be $K_{50} = 1.5 \pm 0.1$ (1.5 ± 0.2) for the high $E_{\mathrm{T}}^{\mathrm{miss}}$ (high H_T) signal region. The second correction factor accounts for the W polarization in $\mathrm{t\bar{t}}$ events, as well as detector effects such as hadronic energy scale and is estimated from simulation; this correction is $K_C = 1.4 \pm 0.4$ (1.3 ± 0.4) for the high $E_{\mathrm{T}}^{\mathrm{miss}}$ (high H_T) signal region.

To translate the top prediction in the $ee, e\mu, \mu\mu$ channels into a prediction for the $e\tau_h, \mu\tau_h$ channels we use a third correction factor estimated from simulation $K_\tau = 0.18 \pm 0.02$ ($k_\tau = 0.18 \pm 0.02$) that accounts for the different lepton acceptances and efficiencies and is derived from simulation. Note that this procedure predicts yields for dileptonic $\mathrm{t\bar{t}}$ decays. Semileptonic $\mathrm{t\bar{t}}$ decays where one quark or gluon jet is misidentified as a τ_h are described in the following section.

7.1.2 Backgrounds with Misidentified Taus

The background with a reconstructed τ_h originating from a misidentified jet or a secondary decay is determined using a tight-to-loose (TL) ratio (or "fake-rate") for τ_hs measured in a background (di-jet) dominated data sample, defined as $H_{\mathrm{T}} > 200$ GeV and $E_{\mathrm{T}}^{\mathrm{miss}} < 20$ GeV. We define tight candidates to pass the full τ_h selection criteria. For the definition of loose candidates we replace the HPS isolation criterium by a loose relative isolation.

The loose tau definition comprises a loosely isolated jet, while the tight definition has to pass the full tau selection. The loose isolation requirement removes any H_{T} dependence of the tight-to-loose ratio, thus the measurement can be extrapolated to the signal regions.

To determine the number of expected events including jets misidentified as τ_hs in the signal region, the identification for one τ_h is loosened. The obtained signal yields are multiplied with the probability that this particular τ_h candidate did not originate from a τ, but passes the tight τ_h selection, P_{fake}:

$$P_{\mathrm{fake}}(p_T, \eta) = \frac{TL(p_T, \eta)}{1 - TL(p_T, \eta)}.$$

A summation over P_{fake} evaluated for all τ_h candidates that pass the loose but not the tight selection gives the final background prediction in each signal region.

The method is tested in a top simulation, where we find agreement within 15%. We correct for a 5% bias observed in top-simulation and assign a 15% systematic uncertainty on the background prediction from the tight-to-loose ratio.

7.2 Results

The data is displayed in the plane of $E_{\mathrm{T}}^{\mathrm{miss}}$ vs. H_T in Fig. 2. Shadowed regions correspond to the the two signal regions. Table 4 summarizes the number of observed data events, the number of SM background events estimated using background techniques described in Sec. 7.1.1 and 7.1.2 as well as predicted yields from simulation.

We find 8 (11) events in the high $E_{\mathrm{T}}^{\mathrm{miss}}$ (high H_T) signal regions, consistent with the background expectations . For the high $E_{\mathrm{T}}^{\mathrm{miss}}$ (high H_T) signal regions we predict a top background yield of $5.9 \pm 1.5_{stat.} \pm 1.9_{syst.}$ ($7.2 \pm 1.6_{stat.} \pm 2.7_{syst.}$) events. For the high $E_{\mathrm{T}}^{\mathrm{miss}}$ (high H_T) signal regions we predict a non-prompt background yield of $1.6 \pm 0.6_{stat.} \pm 0.2_{syst.}$ ($2.9 \pm 0.7_{stat.} \pm 0.4_{syst.}$) events.

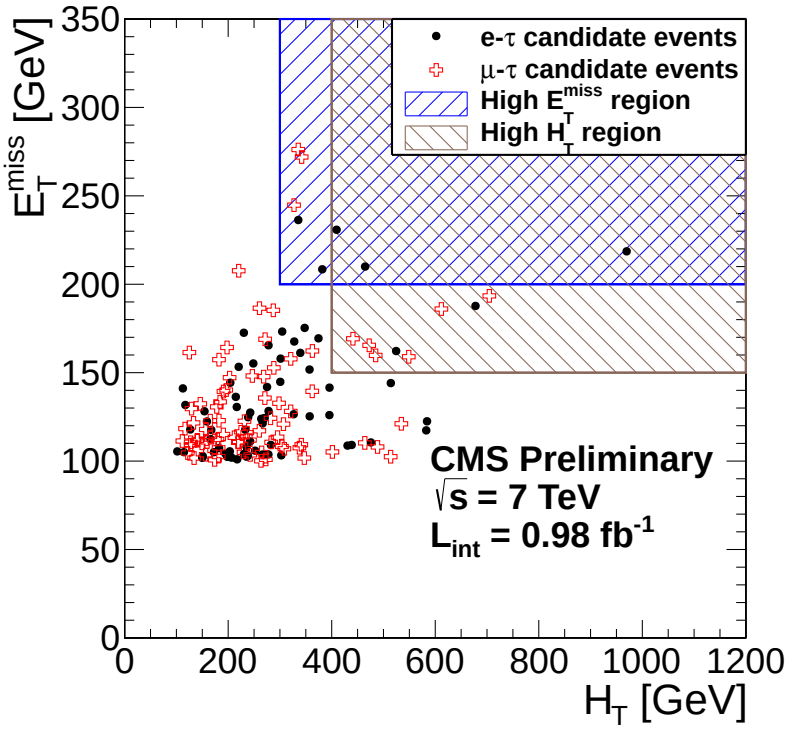

Figure 2: Distributions of $E_{\mathrm{T}}^{\mathrm{miss}}$ vs. H_{T} for data. The high $E_{\mathrm{T}}^{\mathrm{miss}}$ (high H_T) signal region is indicated with the blue dotted (red striped) region.

8 Double Hadronic Tau Final State

8.1 Event Selection

As mentioned above, candidate events for the $\tau_h\tau_h$ final state are selected using a trigger that requires significant $\not{H}_{\mathrm{T}}$, $\not{H}_{\mathrm{T}} > 200$ GeV. The trigger efficiency with respect to events passing offline selections is approximately 98% for $\not{H}_{\mathrm{T}} > 200$ GeV and is measured using a sample of candidate events selected with $l + \tau_h$ triggers that are unbiased to $E_{\mathrm{T}}^{\mathrm{miss}}$ or $\not{H}_{\mathrm{T}}$.

Tau candidates are required to satisfy the following kinematical selection : $p_T > 15$ GeV and $|\eta| < 2.1$. Events are required to have ≥ 2 τ_hs passing the kinematical selections and HPS tau tagging criteria outlined in Sec. 5. For the case of QCD, any non-zero measurements of $\not{H}_{\mathrm{T}}$ arise due to large mismeasurements in the jet energies. Therefore, the $\overrightarrow{\not{H}_{\mathrm{T}}}$ and next-to-leading jet are expected to be mostly back-to-back. QCD dijet events are rejected by applying a requirement on the difference in the azimuth ϕ between the next-to-leading jet and the $\overrightarrow{\not{H}_{\mathrm{T}}}$, $|\Delta\phi(j_2, \not{H}_{\mathrm{T}})| > 0.5$. Finally, events are required to have at least one $\tau_h\tau_h$ pair that is well separated in η–ϕ space, $\Delta R(\tau_{h,i}, \tau_{h,j}) > 0.3$.

8.2 Background Extraction

8.2.1 $t\bar{t}$ Estimation

To estimate the $t\bar{t}$ contribution in the signal region, a control sample is obtained by removing the τ_h isolation requirement and requiring the presence of ≥ 2 jets tagged as b-jets using the track counting high efficiency (TCHE) algorithm [30]. Because QCD, W + jets, and $Z \to \nu\bar{\nu}$ + jets processes are unlikely to contain two b-jets, the requirement of ≥ 2 jets tagged as b-jets provides

Table 4: Summary of the observed and predicted yields in the 2 signal regions. The systematic uncertainties on the $p_T(\ell\ell)$ and TL ratio method predictions are discussed in the text. "$\sum$MC True" indicates the sum of SM backgrounds including a real hadronic τ decay (dominated by dileptonic $t\bar{t}$), "$\sum$MC Fake" indicates SM processes with a jet misidentified as hadronic τ and "$\sum$SM MC" is the sum of both contributions. The LM1, LM2 and LM13 yields include uncertainties from MC statistics, trigger efficiency, lepton selection efficiency, hadronic energy scale and integrated luminosity.

Sample	High H_{T}	High $E_{\mathrm{T}}^{\mathrm{miss}}$
$\sum$MC True	$4.1 \pm 0.6_{stat.} \pm 1.3_{syst.}$	$2.7 \pm 0.5_{stat.} \pm 0.9_{syst.}$
$\sum$MC Fake	$6.0 \pm 3.8_{stat.} \pm 1.9_{syst.}$	$6.9 \pm 4.2_{stat.} \pm 2.2_{syst.}$
$\sum SM$ MC	$10.0 \pm 3.8_{stat.} \pm 3.3_{syst.}$	$9.6 \pm 4.2_{stat.} \pm 3.1_{syst.}$
$p_T(\ell\ell)$Prediction	$7.2 \pm 1.6_{stat.} \pm 2.7_{syst.}$	$5.9 \pm 1.5_{stat.} \pm 1.9_{syst.}$
TL Prediction	$2.9 \pm 0.7_{stat.} \pm 0.4_{syst.}$	$1.6 \pm 0.6_{stat.} \pm 0.2_{syst.}$
$\sum$Prediction from data	$10.1 \pm 1.7_{stat.} \pm 2.7_{syst.}$	$7.5 \pm 1.6_{stat.} \pm 1.9_{syst.}$
Data	11	8
$LM1$	$17.3 \pm 0.7_{stat.} \pm 5.3_{syst.}$	$15.8 \pm 0.7_{stat.} \pm 4.9_{syst.}$
$LM2$	$3.1 \pm 0.1_{stat.} \pm 1.0_{syst.}$	$3.0 \pm 0.1_{stat.} \pm 0.9_{syst.}$
$LM13$	$40.8 \pm 2.7_{stat.} \pm 12.6_{syst.}$	$32.3 \pm 2.4_{stat.} \pm 10.0_{syst.}$

a control sample with $\sim 99\%$ purity of $t\bar{t}$ events, $N_{t\bar{t}}^{pure}$, where the probability/efficiency to find ≥ 2 τ_hs/jets passing the isolation criteria is measured. The measurent of the isolation efficiency, $\varepsilon^{\tau_h \text{ isolation}}$, combined with the probability to identify two b-jets, $P(2\ b\text{-jets})$, determines the $t\bar{t}$ contribution in the signal region:

$$N_{t\bar{t}}^{Signal} = N_{t\bar{t}}^{pure} \frac{1}{P(2\ b\text{-jets})} \varepsilon^{\tau_h \text{ isolation}}.$$

The isolation efficiency τ_h is measured by determining the percentage of events from the $t\bar{t}$ control sample with at least two τ_h objects passing the isolation requirements. The b-tagging efficiency as measured in [30] is used to determine the probability to tag ≥ 2 b-jets. Cross-checks are made to validate the use of the b-tagging efficiency as measured in [30] for this analysis. This is done by using a high multiplicity jet selection to obtain a semi-clean sample of $t\bar{t}$ events where the b-tagging efficiency used to calculate $P(2\ b\text{-jets})$ is measured and required to be consistent with the value as measured in [30]. The H_T distribution for events in the $t\bar{t}$ control sample is shown in Fig. 3a.

8.2.2 QCD Estimation

QCD contributes to the signal region due to mismeasurements in the jet energies, which leads to large values of $\not{H}_{\mathrm{T}}$, and jets misidentified as τ_hs. Therefore, the QCD contribution is estimated by removing the τ_h isolation criteria and inverting the $|\Delta\phi(j_2, \not{H}_{\mathrm{T}})|$ requirement to obtain a high purity QCD enriched sample where correction factors are obtained and used to determine the signal contribution. Fig. 3b shows the expected and observed $\Delta\phi(j_2, \not{H}_{\mathrm{T}})$ distributions. The requirement of $|\Delta\phi(j_2, \not{H}_{\mathrm{T}})| < 0.15$ is used to obtain a control sample enriched with a high purity of QCD events where a data-MC scale factor is obtained, $f_{QCD} = \frac{N_{Data}^{control}}{N_{Simulation}^{control}}$, and used to correct the signal prediction for QCD in simulation:

$$N^{Signal}_{QCD-Data} = f_{QCD} \cdot N^{Signal}_{QCD-MC}.$$

8.2.3 $Z \to \nu\bar{\nu}$ + Jets Estimation

Because a high purity sample of $Z \to \nu\bar{\nu}$ + jets events cannot be obtained without significant modifications to the signal selections, the contribution from $Z \to \nu\bar{\nu}$ + jets is determined by using similar jet and $E_{\mathrm{T}}^{\mathrm{miss}}$ selections to the final analysis path, but requiring the presence of two clean muons to select $Z \to \mu\mu$ + jets and treating the muons as neutrinos in order to properly model the large $\not{H}_{\mathrm{T}}$ values associated with $Z \to \nu\bar{\nu}$ + jets events. Obtaining a clean sample of $Z \to \mu^+\mu^-$ + jets is much easier due to the much lower probability for a jet to be misidentified as a muon compared to the jet$\to \tau_h$ misidentification rates. The $\not{H}_{\mathrm{T}}$ distribution for events passing this criteria is shown in Fig. 3c. The control sample is enriched with $\sim 99\%$ purity of $Z \to \mu\mu$ + jets events. Once a high purity sample of $Z \to \mu^+\mu^-$ + jets is obtained ($N^{pure}_{Z\to\mu^+\mu^-+Jets}$), efficiencies for $Z \to \nu\bar{\nu}$ + jets events are measured and the number of observed events are corrected for the muon acceptance (A_μ), identification (ε_μ) efficiencies and branching ratios to muons, $B(Z \to \mu^+\mu^-)$, in order to determine the $Z \to \nu\bar{\nu}$ + jets expected contribution in the signal region:

$$N_{Z\to\nu\bar{\nu}+Jets} = \frac{N^{pure}_{Z\to\mu^+\mu^-+Jets}}{A_\mu \varepsilon^2_\mu} \frac{B(Z \to \nu\bar{\nu})}{B(Z \to \mu^+\mu^-)} \varepsilon^{\not{H}_{\mathrm{T}}} \varepsilon^{\tau\ \mathrm{ID}}.$$

8.2.4 W + Jets Estimation

The W+jets contribution is estimated by removing the requirements on τ_h isolation, maintaining the $|\Delta\phi(j_2, \not{H}_{\mathrm{T}})| > 0.5$ requirement to minimize QCD, and requiring zero jets tagged as b-jets to minimize the presence of $t\bar{t}$. However, with these requirements, the purity of W + jets events is only $\sim 65\%$. Therefore, the non-negligible contributions from QCD, $t\bar{t}$, and $Z \to \nu\bar{\nu}$ + jets in the W + jets enhanced region is subtracted from the observed data. The non-negligible contributions from QCD, $t\bar{t}$, and $Z \to \nu\bar{\nu}$ + jets in the W + jets enhanced region are determined by extrapolating from their respective control regions using similar methodologies as those described above. Fig. 3d shows the resultant $\not{E}_{\mathrm{T}}$ distribution after the subtraction techniques have been employed. The estimation for W+jets in the signal region is obtained by determining the probability to tag zero jets as b-jets and measuring the probability to find ≥ 2 τ_h/jets passing the isolation criteria, $\varepsilon^{\tau_h\ \mathrm{isolation}}$:

$$N^{W+Jets}_{signal} = \frac{N^{W+Jets\ \mathrm{enhanced}}_{W+Jets} \times \varepsilon^{\tau_h\ \mathrm{Isolation}}}{P_{b-Tagging}(0)}.$$

The efficiency $\varepsilon^{\tau_h\ \mathrm{Isolation}}$ is measured by determining the percentage of events from the W+jets control sample, after subtraction of other backgrounds, with at least two τ_h objects passing the isolation requirements. The b-tagging efficiency as measured in [30] is used to determine the probability to tag 0 b-jets.

8.3 Results

Table 5 shows the observed events in data as well as the estimated SM backgrounds in the signal region. As expected, the largest background source is from $t\bar{t}$ due to the presence of high momentum imbalance due to the neutrinos from the W decays, high p_T jets from the

decay of the top quarks and hadronic decay of the W, and real or misidentified τ_h from the hadronic decay of the W. The estimations for SM background processes are in good agreement with the number of observed events in the signal region. In order to test the robustness of the background estimation methods and further ensure the SM signal estimations are well modeled, we define a "loose" preselection region where the isolation criteria on the tau legs is removed in order to obtain a high statistics sample. Table 5 shows the predicted rates and observed number of events in this "loose" preselection region. The expected contributions for the cMSSM benchmark points $LM1$, $LM2$, and $LM13$ are shown. Figures 4a– 4d show the $\not{E}_{\mathrm{T}}$, $\not{H}_{\mathrm{T}}$, $M_{\tau\tau}^{LS}$, and $\Delta\phi(j_1, \not{H}_{\mathrm{T}})$ distributions in the "loose" preselection region.

Table 5: Number of observed data events and predicted background rates.

Process	"Loose" $\tau\tau$ Preselection Region	Signal Region
QCD	213.8 ± 5.9	$0.58 \pm 0.02_{stat} \pm 0.41_{syst}$
$W + Jets$	993.1 ± 21.3	$0.00 \pm 1.20_{stat} \pm 0.10_{syst}$
$t\bar{t}$	547.5 ± 43.8	$2.18 \pm 2.18_{stat} \pm 0.35_{syst}$
$Z \to \nu\bar{\nu} + Jets$	574.6 ± 47.2	$0.00 \pm 0.16_{stat} \pm 0.02_{syst}$
$\sum SM$	2329.0 ± 68.1	$2.76 \pm 2.50_{stat} \pm 0.55_{syst}$
Observed $Data$	2165	3
$LM1$	$1862.7 \pm 5.63_{stat} \pm 558.81_{syst}$	$10.76 \pm 0.52_{stat} \pm 3.23_{syst}$
$LM2$	$289.8 \pm 1.77_{stat} \pm 86.94_{syst}$	$7.99 \pm 0.24_{stat} \pm 2.40_{syst}$
$LM13$	$2286.0 \pm 7.64_{stat} \pm 685.80_{syst}$	$31.07 \pm 1.06_{stat} \pm 9.32_{syst}$

9 Additional Information for Model Testing

Other models of new physics in the di-tau final state can be probed in an approximate way by simple generator-level studies using the lepton efficiencies, and the detector responses for H_{T} and $E_{\mathrm{T}}^{\mathrm{miss}}$. The leptonic trigger efficiencies for events containing $e\tau_h$ and $\mu\tau_h$ is $\sim 90\%$ [20]. The hadronic trigger efficiency used for $\tau_h\tau_h$ finale state is 98%. The muon identification efficiency is $\approx$ 96%; the electron identification efficiency varies approximately linearly from $\approx$ 60% at $p_{\mathrm{T}} = 10$ GeV to 90% for $p_{\mathrm{T}} > 30$ GeV.

The tau identification efficiency varies approximately linearly from $\approx 30\%$ at $p_{\mathrm{T}} = 20$ GeV to 38% for $p_{\mathrm{T}} > 50$ GeV. Since isolation is an integral part of the tau identification it is included here.

The light lepton isolation efficiency depends on the lepton momentum, as well as on the jet activity in the event. In $t\bar{t}$ events, it varies approximately linearly from $\approx$ 73% (muons) and $\approx$ 82% (and electrons) at $p_{\mathrm{T}} = 10$ GeV to $\approx$ 97% for $p_{\mathrm{T}} > 60$ GeV. In LM1 events, this efficiency is decreased by $\approx$5–10% over the whole momentum spectrum.

The average detector responses (the reconstructed quantity divided by the generated quantity) for H_{T} and $E_{\mathrm{T}}^{\mathrm{miss}}$ are consistent with unity within the 7.5% jet energy scale uncertainty. The experimental resolutions on these quantities are 9% and 12%, respectively.

10 Limits on New Physics

For all regions, we find reasonable agreement between the observed yields and the predictions from simulation and data-driven methods. We set upper limits on the non-SM contributions to the signal regions of e/μ τ_h, τ_h τ_h and their combination.

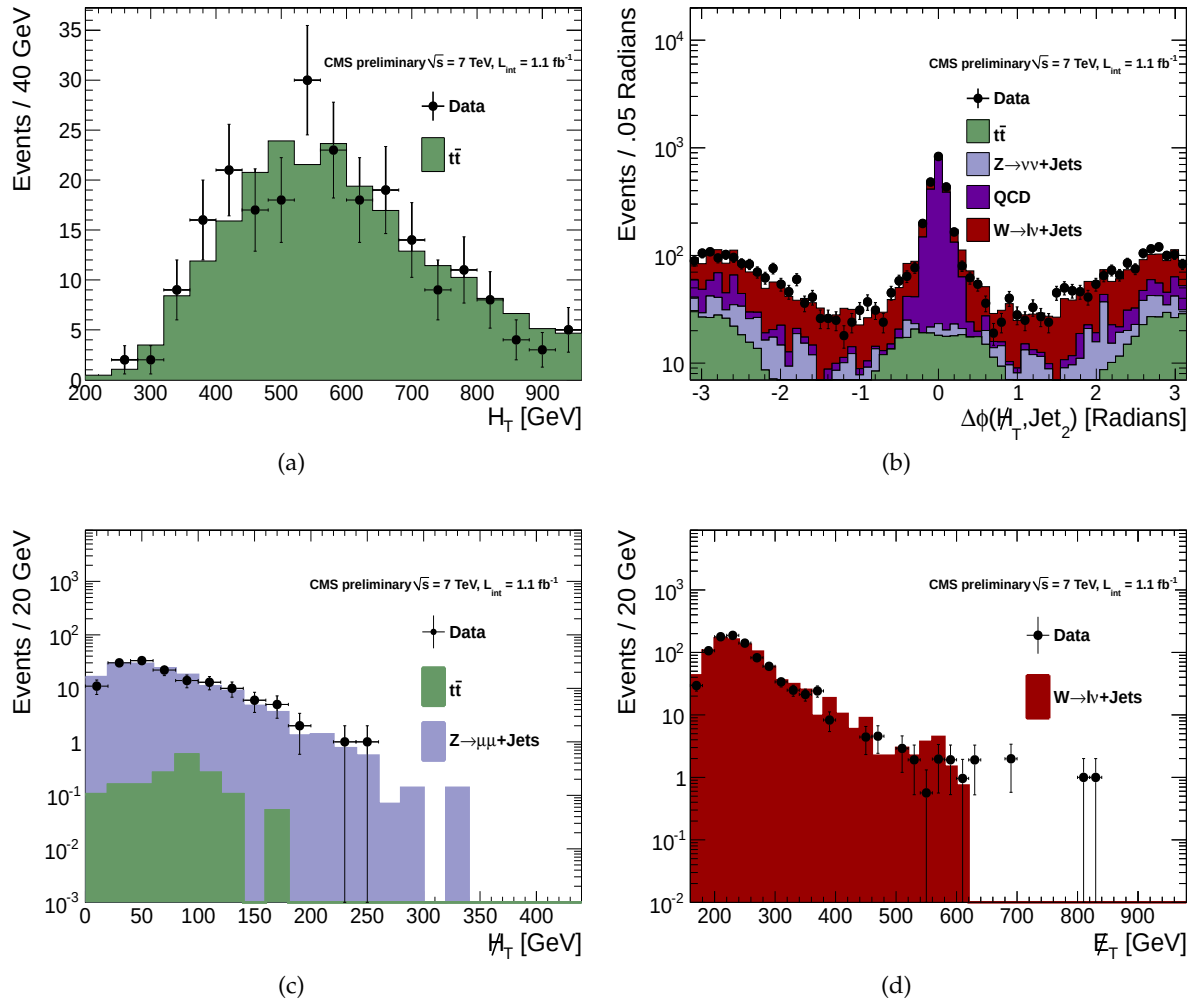

Figure 3: (a) H_T distribution in the $t\bar{t}$ control region. (b) Standard Model background enhanced sample depicting the effectiveness of $|\Delta\phi(\not{H}_T, j_2)| < 0.15$ in selecting a high purity sample of QCD events. (c) $\not{H}_T$ distribution in the $Z \to \mu\mu$ + jets control region used to estimate $Z \to \nu\nu$ + jets. (d) $\not{E}_T$ distribution in the W + jets control region after subtraction of all other backgrounds.

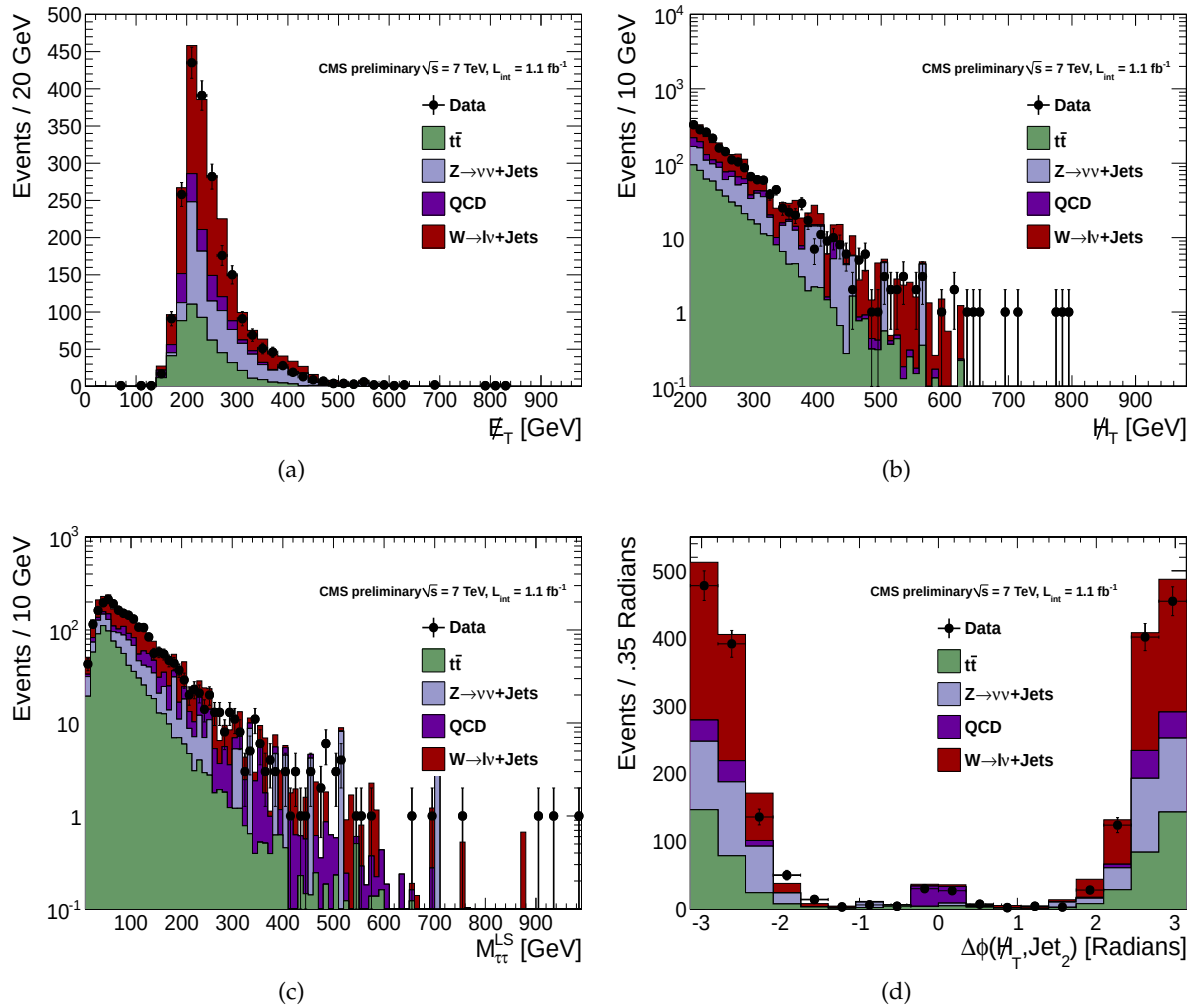

Figure 4: (a) $\not\!\!E_{\mathrm{T}}$, (b) $\not\!\!H_{\mathrm{T}}$, (c) $M_{\tau\tau}^{LS}$, and (d) $\Delta\phi(j_1, \not\!\!H_{\mathrm{T}})$ in a "loose" signal region without requiring τ_h isolation to enhance the statistics and compare the data-driven estimation of backgrounds with the observed distributions from data.

The results of the counting experiments in the signal regions are also used to place model-dependent limits on the cross-section.We place 95% confidence level (CL) upper limits (UL) using a hybrid frequentist-bayesian CL_S method [31] on the cross section, and compare these limits to the expected values of this quantity for the benchmark SUSY scenarios. The CL_S method compares the result of the experiment with the expectations for signal plus background (s+b) and background only (b) hypotheses. In order to test the compatibility of the data with the signal plus background and background only hypotheses, the confidence levels CL_{s+b} and CL_b are constructed. These confidence levels are defined as

$$CL_{s+b} = \mathcal{P}(\text{data}|s+b) = \prod_{i=1}^{\text{nbins}} \frac{(s_i+b_i)^{n_i} e^{-(s_i+b_i)}}{n_i!} \tag{2}$$

and

$$CL_b = \mathcal{P}(\text{data}|b) = \prod_{i=1}^{\text{nbins}} \frac{b_i^{n_i} e^{-b_i}}{n_i!}. \tag{3}$$

The results are summarized in Table 6, which indicates that all benchmark SUSY scenarios are ruled out by these results. The systematic uncertainties are incorporated as nuisance parameters, which are generated according to log normal and Gaussian distributions. The combination of the channels is done taking into account the correlations in the uncertainties.

Table 6: Summary of model-dependent limits. The efficiency and acceptance are defined in the text; the efficiency uncertainty is dominated by the uncertainty in the hadronic energy scale. The CL_S 95% CL UL on the cross section is indicated, as well as the value of this quantity for the LM1, LM2 and LM13 scenarios.

high H_T signal region (e/μ τ_h)	LM1	LM2	LM13
UL $\sigma^{CL_S^{95\%}}_{expected}$ [pb]	3.8 ± 1.9	2.6 ± 1.2	2.1 ± 1.5
UL $\sigma^{CL_S^{95\%}}_{measured}$ [pb]	4.2	2.9	2.5
high E_T^{miss} signal region (e/μ τ_h)	LM1	LM2	LM13
UL $\sigma^{CL_S^{95\%}}_{expected}$ [pb]	3.3 ± 1.9	2.3 ± 1.1	2.3 ± 1.5
UL $\sigma^{CL_S^{95\%}}_{measured}$ [pb]	3.7	2.5	2.6
τ_h τ_h	LM1	LM2	LM13
UL $\sigma^{CL_S^{95\%}}_{expected}$ [pb]	3.9 ± 1.9	0.6 ± 0.3	1.8 ± 1.2
UL $\sigma^{CL_S^{95\%}}_{measured}$ [pb]	4.2	0.7	2.0
high H_T signal region (e/μ τ_h) and τ_h τ_h	LM1	LM2	LM13
UL $\sigma^{CL_S^{95\%}}_{expected}$ [pb]	2.5 ± 1.5	0.6 ± 0.3	1.2 ± 1.0
UL $\sigma^{CL_S^{95\%}}_{measured}$ [pb]	2.9	0.7	1.5
high E_T^{miss} signal region (e/μ τ_h) and τ_h τ_h	LM1	LM2	LM13
UL $\sigma^{CL_S^{95\%}}_{expected}$ [pb]	2.4 ± 1.4	0.6 ± 0.3	1.2 ± 1.0
UL $\sigma^{CL_S^{95\%}}_{measured}$ [pb]	2.8	0.6	1.5
σ^{NLO}_{model} [pb]	6.6	0.8	9.8

11 Summary

We have presented a search for BSM physics using final states with opposite-sign tau pairs using a data sample of proton-proton collisions at 7 TeV centre-of-mass energy corresponding to an integrated luminosity of up to 1.1 fb^{-1}, recorded by the CMS detector in 2011. Two complementary search strategies were performed and we conclude that no evidence for non-SM contributions to the signal regions is observed. In the absence of evidence for BSM physics, we have set upper limits on the non-SM contributions. Additional information was provided to allow testing whether specific models of new physics are excluded by these results.

References

[1] D. Spergel et al. *Astrophys. J. Suppl. Ser. 148, 175* (2003).

[2] S. P. Martin, "A Supersymmetry primer", arXiv:hep-ph/9709356.

[3] J. Wess and B. Zumino, "Supergauge Transformations in Four-Dimensions", *Nucl.Phys.* **B70** (1974) 39–50. doi:10.1016/0550-3213(74)90355-1.

[4] R. Arnowitt et al. *Phys. Rev. 49, 970* (1982).

[5] L. Hall et al. *Phys. Rev. D 27, 2359* (1983).

[6] CMS Collaboration, "CMS technical design report, volume II: Physics performance", *J. Phys. G* **34** (2007) 995–1579. doi:10.1088/0954-3899/34/6/S01.

[7] CMS Collaboration, "Search for supersymmetry in events with opposite-sign dileptons and missing energy", *CMS Physics Analysis Summary* **CMS-PAS-SUS-11-011** (2011).

[8] A. Bresking et al., "The CERN Large Handron Collider: Accelerator and Experiments", *CERN Publication* **Vol 2** (2009).

[9] CMS Collaboration, "The CMS experiment at the CERN LHC", *J. Instrum. 0803:S08004* (2008).

[10] T. Sjostrand, S. Mrenna, and P. Z. Skands, "PYTHIA 6.4 Physics and Manual", *JHEP* **0605** (2006) 026, arXiv:hep-ph/0603175. doi:10.1088/1126-6708/2006/05/026.

[11] J. Alwall, "MadGraph/MadEvent v4: The New Web Generation", *JHEP* **2007** (2007) 028. doi:10.1088/1126-6708/2007/09/028.

[12] Z. Was et al., "TAUOLA the library for tau lepton decay", *arXiv:hep-ph/0011305v1* (2000).

[13] GEANT4 Collaboration, "GEANT4: A Simulation toolkit", *Nucl.Instrum.Meth.* **A506** (2003) 250–303. doi:10.1016/S0168-9002(03)01368-8.

[14] M. Cacciari, G. P. Salam, and G. Soyez, "The Anti-k(t) jet clustering algorithm", *JHEP* **0804** (2008) 063, arXiv:0802.1189. doi:10.1088/1126-6708/2008/04/063.

[15] CMS Collaboration, "Commissioning of the Particle-Flow Reconstruction in Minimum-Bias and Jet Events from pp Collisions at 7 TeV", *CMS Physics Analysis Summary* **CMS-PAS-PFT-10-002** (2010).

[16] CMS Collaboration Collaboration, "First Measurement of the Cross Section for Top-Quark Pair Production in Proton-Proton Collisions at sqrt(s)=7 TeV", *Phys.Lett.* **B695** (2011) 424–443, arXiv:1010.5994. doi:10.1016/j.physletb.2010.11.058.

[17] CMS Collaboration, "Particle Flow Event Reconstruction in CMS and Performance for Jets, Taus, and $\not\!\!E_{\mathrm{T}}$", *CMS Physics Analysis Summary CMS-PAS-PFT-09-001* (2009).

[18] CMS Collaboration, "Performance of tau reconstruction algorithms in 2010 data collected with CMS", *CMS Physics Analysis Summary CMS-PAS-TAU-11-001* (2011).

[19] CMS Collaboration, "Measurement of CMS Luminosity", *CMS Physics Analysis Summary* **CMS-PAS-EWK-10-002** (2010).

[20] CMS Collaboration, "Search for Neutral Higgs Bosons Decaying to Tau Pairs in pp Collisions at $\sqrt{s} = 7$ TeV", *CMS Physics Analysis Summary* **CMS-PAS-HIG-11-009** (2011).

[21] P. M. Nadolsky, H.-L. Lai, Q.-H. Cao et al., "Implications of CTEQ global analysis for collider observables", *Phys. Rev.* **D78** (2008) 013004. doi:10.1103/PhysRevD.78.013004.

[22] A. Martin, W. Stirling, R. Thorne et al., "Parton distributions for the LHC", *Eur.Phys.J.* **C63** (2009) 189–285. doi:10.1140/epjc/s10052-009-1072-5.

[23] R. Ball, L. D. Debbio, A. Guffanti et al., "A first unbiased global NLO determination of parton distributions and their uncertainties", arXiv:1002.4407.

[24] G. et al., "How to use SANC to improve the PHOTOS Monte Carlo simulation of bremsstrahlung in leptonic W-Boson decays", *hep-ph/0303260* (2003).

[25] G. M. et al., "W Production in an Improved Parton-Shower Approach", *hep-ph/9812455* (1998).

[26] V. Pavlunin, "Modeling missing transverse energy in V+jets at CERN LHC", *Phys.Rev.* **D81** (2010) 035005, arXiv:0906.5016. doi:10.1103/PhysRevD.81.035005.

[27] J. Aguilar-Saavedra, J. Carvalho, N. F. Castro et al., "Probing anomalous Wtb couplings in top pair decays", *Eur.Phys.J.* **C50** (2007) 519–533, arXiv:hep-ph/0605190. doi:10.1140/epjc/s10052-007-0289-4.

[28] A. Czarnecki, J. G. Korner, and J. H. Piclum, "Helicity fractions of W bosons from top quark decays at NNLO in QCD", *Phys.Rev.* **D81** (2010) 111503, arXiv:1005.2625. doi:10.1103/PhysRevD.81.111503.

[29] CMS Collaboration Collaboration, "Search for Physics Beyond the Standard Model in Opposite-Sign Dilepton Events at $\sqrt{s} = 7$ TeV", arXiv:1103.1348. * Temporary entry *.

[30] CMS Collaboration, "Performance of b-jet identification in CMS", *CMS Physics Analysis Summary* **CMS-PAS-BTV-11-001** (2011).

[31] Particle Data Group Collaboration, "Review of particle physics", *J. Phys.* **G 37** (2010) 075021. doi:10.1088/0954-3899/37/7A/075021.